

# Structural, electronic and phononic properties of PtSe<sub>2</sub>: from monolayer to bulk

A Kandemir<sup>1</sup> , B Akbali<sup>2</sup>, Z Kahraman<sup>3</sup>, S V Badalov<sup>3</sup> , M Ozcan<sup>3</sup>,  
F Iyikanat<sup>2</sup>  and H Sahin<sup>3,4</sup> 

<sup>1</sup> Department of Materials Science and Engineering, Izmir Institute of Technology, 35430, Izmir, Turkey

<sup>2</sup> Department of Physics, Izmir Institute of Technology, 35430, Izmir, Turkey

<sup>3</sup> Department of Photonics, Izmir Institute of Technology, 35430, Izmir, Turkey

<sup>4</sup> ICTP-ECAR Eurasian Center for Advanced Research, Izmir Institute of Technology, 35430, Izmir, Turkey

E-mail: [alikandemir@iyte.edu.tr](mailto:alikandemir@iyte.edu.tr)

Received 11 April 2018, revised 19 May 2018

Accepted for publication 11 June 2018

Published 29 June 2018



CrossMark

## Abstract

The layer dependent structural, electronic and vibrational properties of the 1T phase of two dimensional (2D) platinum diselenide are investigated by means of state-of-the-art first-principles calculations. The main findings of the study are: (i) monolayer platinum diselenide has a dynamically stable 2D octahedral structure with 1.66 eV indirect band gap, (ii) the semiconducting nature of 1T-PtSe<sub>2</sub> monolayers remains unaffected even at high biaxial strains, (iii) top-to-top (AA) arrangement is found to be energetically the most favorable stacking of 1T-PtSe<sub>2</sub> layers, (iv) the lattice constant (layer-layer distance) increases (decreases) with increasing number of layers, (v) while monolayer and bilayer 1T-PtSe<sub>2</sub> are indirect semiconductors, bulk and few-layered 1T-PtSe<sub>2</sub> are metals, (vi) Raman intensity and peak positions of the A<sub>1g</sub> and E<sub>g</sub> modes are found to be highly dependent on the layer thickness of the material, hence; the number of layers of the material can be determined via Raman measurements.

Keywords: 2D materials, monolayer PtSe<sub>2</sub>, monolayer-to-bulk properties, Raman, semiconductor-metal transition

(Some figures may appear in colour only in the online journal)

## 1. Introduction

Layered materials stacked with weak out-of-plane van der Waals (vdW) interactions, have aroused considerable interest for many decades [1, 2]. In addition, advances in the synthesis techniques of layered two dimensional (2D) materials have also led to the emergence of a variety of monolayer crystals such as graphene [3], transition metal dichalcogenides (TMDs) [4], post-transition metal chalcogenides (PTMCs) [5], h-BN [6, 7], h-AlN [8], silicene [9, 10] and metal hydroxides [11, 12].

In the family of 2D materials, TMDs are desirable both for fundamental research and technological advancement thanks to their interesting optical and electrical properties, and their mechanical stability [13–18]. Dichalcogenides of Mo and W, the most popular materials among TMDs, have

received considerable interest due to their exceptional physical properties such as  $\approx 250 \text{ cm}^2 \text{ V}^{-1} \text{ s}^{-1}$  room temperature mobility, excellent on/off ratio ( $\sim 10^8$ ), thickness dependent metallic and semiconducting behavior, tunable band gaps, and controllable topological electronic properties [5, 19–22].

Among TMDs, apart from well-known Mo and W dichalcogenides, lamellar crystals of Pt dichalcogenides have also attracted interest due to their semi-metallic electronic structure [23, 24], high optoelectronic performance [25], and enhanced photocatalytic activities [26, 27]. Besides their bulk form, 2D Pt dichalcogenides are promising materials for nanoelectronic device applications due to their intriguing electronic properties such as the transition from metal to semiconductor [28–30]. It has been shown that few-layer PtS<sub>2</sub> phototransistors exhibit a very high responsivity reaching  $1.56 \times 10^3 \text{ A W}^{-1}$  [31]. In addition, Zhao *et al* reported that

few-layer PtSe<sub>2</sub> field effect transistors (FETs) exhibit high electron mobility at room-temperature ( $\approx 210 \text{ cm}^2 \text{ V}^{-1} \text{ s}^{-1}$ ) on an SiO<sub>2</sub>/Si substrate [32]. Chia *et al* investigated the correlation between varying chalcogen types to the electrochemical and catalytic performances of Pt dichalcogenides [33]. Very recently, it was revealed that a vertically aligned PtSe<sub>2</sub>/GaAs heterojunction shows broad sensitivity to illumination ranging from deep ultraviolet (UV) to near-infrared (NIR) light [34]. Similarly it was shown that multilayer PtSe<sub>2</sub>/FA<sub>0.85</sub> Cs<sub>0.15</sub> PbI<sub>3</sub> perovskite heterojunction photodetectors are ultrafast, self-driven and air-stable and also exhibited high sensitivity to illumination ranging from the UV to NIR spectrum region [35]. Sattar *et al* reported that monolayer and bilayer PtSe<sub>2</sub> form n-type and p-type Schottky contacts with graphene, respectively [36]. Sajjad *et al* demonstrated that monolayer 1T-PtSe<sub>2</sub> is a good candidate for gas sensor applications due to high adsorption energy and robust character of the band edges of the electronic band structure [37]. Furthermore, Yao *et al* investigated that centrosymmetric monolayer PtSe<sub>2</sub> thin film exhibits R-2 Rashba effect and intrinsic spin-layer locking [38]. In the very recent study Ciarrocchi *et al* showed that high electrical conductivity and efficient transistor operations can be achieved by using only PtSe<sub>2</sub> material by varying the thickness from 14 to 2 nm [39].

In this study, motivated by the recent studies revealing the superior optoelectronic properties of TMDs, we present a comprehensive investigation on the thickness-dependent characteristics of 1T-PtSe<sub>2</sub> by performing state of the art first-principles calculations. The paper is organized as follows: details of the computational methodology are given in section 2. The structural, electronic and vibrational properties of the 1T-PtSe<sub>2</sub> monolayer are discussed in section 3. In section 4, the effect of dimensional crossover on electronic and vibrational characteristics is examined. Finally, our results are discussed in section 5.

## 2. Computational methodology

The *ab initio* calculations were performed within the density functional theory (DFT) formalism by using the Vienna *ab initio* Simulation Package (VASP) [40, 41]. Calculations were performed using the spin-polarized generalized gradient approximation (GGA) of Perdew-Burke-Ernzerhof (PBE) functional [42]. Correction for the van der Waals (vdW) to the PBE functional was done with using the DFT-D2 method of Grimme [43].

The kinetic energy cutoff for a plane-wave basis set was taken as 500 eV. The convergence criterion of self-consistent calculations for ionic relaxations was  $10^{-6}$  eV between two consecutive steps and the total force of the all atoms in the unit cell was reduced to a value of less than  $10^{-5}$  eV/Å. Pressures on the used lattice unit cells were decreased to values less than 1.0 kbar. To hinder interactions between the adjacent cells along the *z*-direction, at least 14 Å vacuum space was used. Analysis of the charge transfers in the structures was determined by using the Bader technique [44].

The vibrational properties were obtained via PHONOPY code [45] that use the finite-displacement method. The cohesive energy per atom  $E_{Coh}$  was calculated by using the formula  $E_{Coh} = [n_{Pt}E_{Pt} + n_{Se}E_{Se} - E_{ML}]/n_{tot}$ , where  $E_{Pt}$  and  $E_{Se}$  represent the energies of single isolated Pt and Se atoms, respectively.  $E_{ML}$  stands for the total energy of the 1T-PtSe<sub>2</sub> structure,  $n_{tot}$ ,  $n_{Pt}$  and  $n_{Se}$  denote the total number of atoms, number of Pt and Se atoms within the unit cell, respectively.

## 3. Monolayer PtSe<sub>2</sub>

For a complete analysis of how the structural, electronic and phononic properties of the PtSe<sub>2</sub> crystal evolve with thickness, we first investigate the characteristics of monolayers comprehensively.

The optimized atomic structure of the octahedral coordination forming the 1T polytype of PtSe<sub>2</sub> belongs to  $P\bar{3}m1$  space group. As shown in figure 1(a), the Bravais lattice of 1T-PtSe<sub>2</sub> monolayer is hexagonal with lattice vectors,  $\vec{a} = 0.5a(\sqrt{3}\hat{x} - \hat{y})$ ,  $\vec{b} = 0.5a(\sqrt{3}\hat{x} + \hat{y})$ ,  $\vec{c} = c\hat{z}$ . 1T-PtSe<sub>2</sub> structure with  $D_{3d}$  point group symmetry is composed of three atomic sub-layers with Pt layer sandwiched between two Se layers. The lattice constant of the primitive unit cell of the monolayer 1T-PtSe<sub>2</sub> structure is calculated to be 3.70 Å which is in perfect agreement with previously reported scanning transmission electron microscopy (STEM) data [46]. The Pt-Se bond length in the 1T phase of PtSe<sub>2</sub> crystal structure is found to be 2.52 Å. Moreover, the thickness, defined as vertical distance between uppermost and lowermost Se layers, of 1T-PtSe<sub>2</sub> monolayer is (2.68 Å) is also close to the reported value of 2.53 Å [46].

It is also found that the monolayer 1T-PtSe<sub>2</sub> is formed by a cohesive energy of 4.43 eV/atom which is comparable to the cohesive energy of MoSe<sub>2</sub> and WSe<sub>2</sub> ( $\sim 4.56$  and  $\sim 5.15$  eV/atom, respectively) [47]. According to Bader charge analysis, there is no net charge transfer between bonded atoms in monolayer 1T-PtSe<sub>2</sub> structure and the bond character is entirely covalent in the monolayer 1T-PtSe<sub>2</sub> structure. In addition, the work function is obtained as 5.36 eV in the monolayer 1T-PtSe<sub>2</sub> which is higher than that of similar dichalcogenides such as MoSe<sub>2</sub> and WSe<sub>2</sub> (4.57 and 4.21 eV, respectively) [48].

However, structures obtained from total energy optimization calculations may not correspond to the ground state structure, therefore; for a reliable analysis on the stability of a structure it is also necessary to examine the dynamical stability via phonon calculations. The phonon dispersion curves of the 1T-PtSe<sub>2</sub> crystal structure are shown in figure 1(b).

For the primitive unit cell of 1T-PtSe<sub>2</sub> composed of 3 atoms, the phonon spectrum includes 9 phonon, 3 acoustic and 6 optical branches. Analysis of lattice dynamics shows that the decomposition of the vibration representation of optical modes at the  $\Gamma$  point is  $\Gamma = 2E_g + 2E_u + A_{1g} + A_{2u}$  for the 1T-PtSe<sub>2</sub> monolayer structure. Optical phonons include two doubly degenerate in-plane vibrational modes at  $169 \text{ cm}^{-1}$  ( $E_g$ ) and  $218 \text{ cm}^{-1}$  ( $E_u$ ), and two singly degenerate

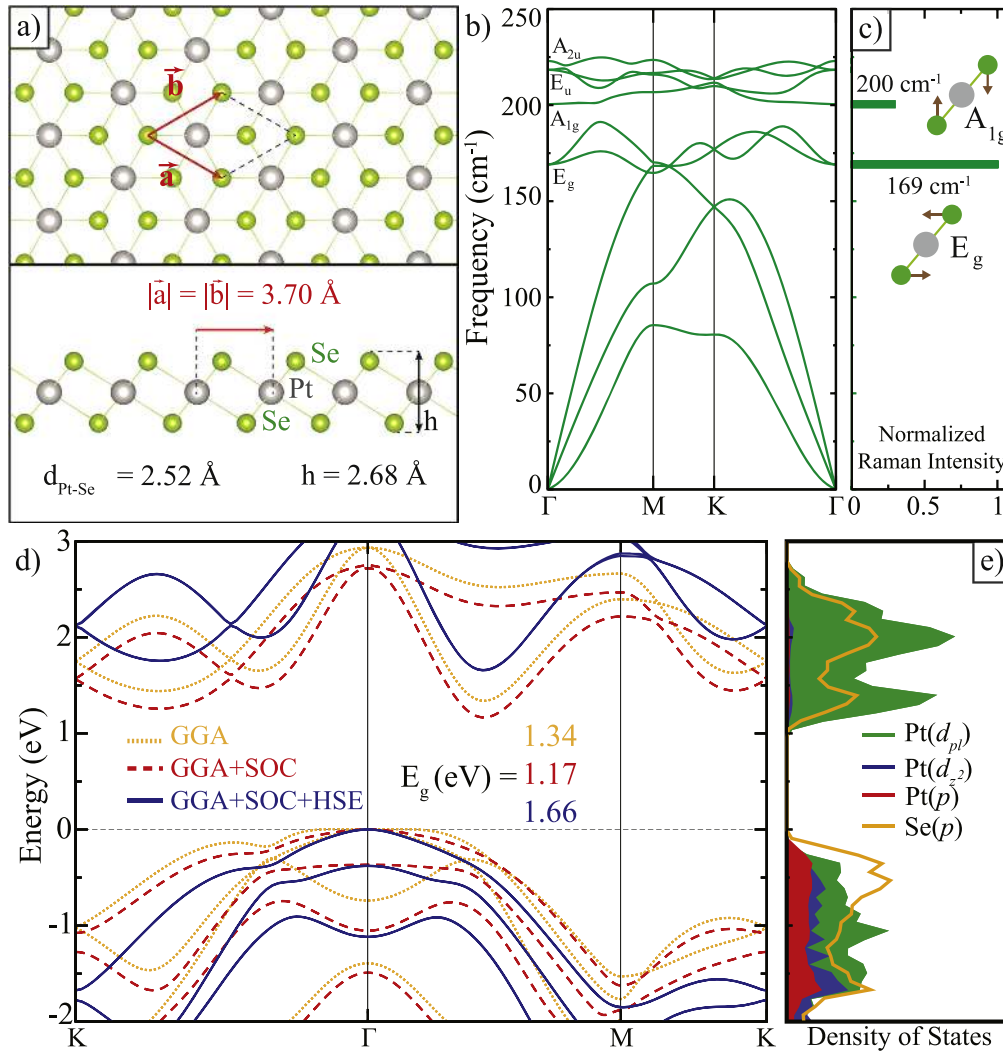


**Figure 1.** (a) Top and side views of geometric structures of 1T-PtSe<sub>2</sub> monolayer. Gray and green atoms show Pt and Se atoms, respectively. (b) The phonon band diagram and (c) normalized Raman intensity of 1T-PtSe<sub>2</sub> monolayer. (d) The electronic band diagram and (e) partial density of states of the monolayer structure. Dotted yellow lines, dashed red lines and solid blue lines show pure GGA, spin-orbit coupling included GGA and hybrid HSE06 functional corrected GGA+SOC results for electronic band dispersions, respectively. The Fermi level is set to zero.

out-of-plane vibrational modes at  $200\text{ cm}^{-1}$  ( $A_{1g}$ ) and  $223\text{ cm}^{-1}$  ( $A_{2u}$ ). Vibrational spectrum through whole the Brillouin Zone indicate that of the 1T-PtSe<sub>2</sub> phase corresponds to a dynamically stable crystal structure. Besides, due to the atomic mass and bonding type of Pt and Se atoms, the phonon modes of 1T-PtSe<sub>2</sub> lie at much lower energies when compared to those of well-known 2D transition metal diselenides, MoSe<sub>2</sub> and WSe<sub>2</sub> [22].

Regarding Raman intensities, in the vibrational spectrum of 1T-PtSe<sub>2</sub>, there are two prominent peaks likely to be observed in experiments. As shown in figure 1(c), (i) one highly intense in-plane  $E_g$  mode at  $169\text{ cm}^{-1}$  and (ii) one moderate intense out-of-plane  $A_{1g}$  mode at  $200\text{ cm}^{-1}$ . Due to the strong covalent character between Pt and Se atoms, out-of-plane motion of the Se atoms has less contribution in the Raman intensity compared to in-plane motion of the Se atoms. Corresponding eigenvectors of the Raman active  $E_g$  and  $A_{1g}$  modes are also sketched in figure 1(c).

As shown in figure 1(d), 1T-PtSe<sub>2</sub> monolayer is an indirect band gap semiconductor with its valence band maximum (VBM) residing at  $\Gamma$  point and conduction band minimum (CBM) within  $\Gamma$ -M point. Calculations with and without spin-orbit interactions and HSE corrections show that the band gaps of 1T-PtSe<sub>2</sub> monolayer are 1.34, 1.17 and 1.66 eV, besides; no change is seen at the band edges of CBM and VBM. With the effect of spin-orbit coupling (SOC), double degenerate VBM is separated at  $\Gamma$  point about 0.4 eV in the 1T-PtSe<sub>2</sub> monolayer and also CBM splits 170 meV at the point between  $\Gamma$  and M. It is seen that HSE correction increases the band gap about 0.5 eV.

As seen in figure 1(e), the calculated orbital projected partial density of states (PDOS) reveals that the valence states are mainly composed of hybridization of  $d$  and  $p$  orbitals of Pt, and  $p$  orbitals of Se atoms. However, the conduction states consist of  $d_{xy}$ ,  $d_{yz}$ ,  $d_{xz}$  and  $d_{x^2-y^2}$  orbitals ( $d_{pl}$ ) of Pt atom and  $p$  orbital of Se atoms. In addition, PDOS shows that  $d$  and  $p$  orbitals of Pt, and  $p$  orbitals of Se are responsible for the

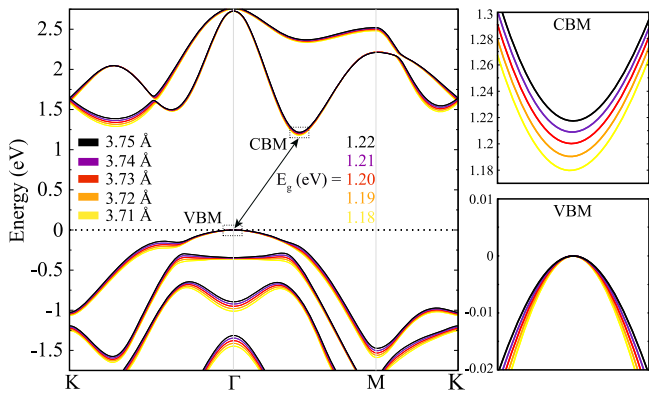


**Figure 2.** The SOC included electronic band diagrams of 1T-PtSe<sub>2</sub> monolayer as a function of tensile biaxial strain. The Fermi level is set to zero. Side views show the valence band maximum (VBM) and conduction band minimum (CBM) on an enlarged scale.

VBM of the monolayer, whereas only  $d_{xy}$ ,  $d_{yz}$ ,  $d_{xz}$  and  $d_{x^2-y^2}$  orbitals ( $d_{pl}$ ) of Pt are dominantly responsible for CBM of the 1T-PtSe<sub>2</sub> structure.

Since the effect of strain due the adjacent layers is inevitable in such lamellar crystal structures, before studying the thickness dependent properties, we investigate the electronic and structural parameters under biaxial strain. Here we apply the strain by scanning the lattice parameters in between monolayer and bulk 1T-PtSe<sub>2</sub>. It is found that the Pt-Se bond length monotonically increases, while the tensile strain rate increases. As seen from figure 2, while VBM at the  $\Gamma$  point is quite insensitive against the biaxial strain, CBM at the  $\Gamma$ -M symmetry point shifts upwards slightly in the energy space. Hence, the reasonable tensile strain causes a slight change in the electronic band gap of the monolayer 1T-PtSe<sub>2</sub> structure. Against tensile deformation, the 1T-PtSe<sub>2</sub> monolayer is a robust semiconductor material which is the essential factor for its utilization in future nanoelectronics.

## 4. Dimensional crossover from monolayer to bulk

### 4.1. Stacking types and thickness-dependence of the atomic structure of 1T-PtSe<sub>2</sub>

Stacking order of the sublayers in a layered material directly determines its structural, vibrational, electronic and optical properties. Therefore, theoretical prediction prior to experimental synthesis of the stacking order is important.

The possible stacking orders in 1T-PtSe<sub>2</sub> crystal are namely AA, (Pt atoms aligned on Pt atoms) AB, (Pt atoms aligned on Se atoms) A'A, (similar to AA but the top layer is upside-down) and A'B (similar to AB but the top layer is upside-down) and are presented in figure 3. It is found that the most energetically favorable stacking order is top to top (AA), as shown in figure 3(a). In addition, AB, A'A, and A'B, stackings are found to be 159, 321 and 91 meV, respectively, less favorable than the ground state structure. The lattice constant of the AA stacked structure, 3.73 Å, is consistent with the experimentally reported value [28]. Furthermore, the interlayer distances are calculated to be 2.14, 2.89, 3.61, and

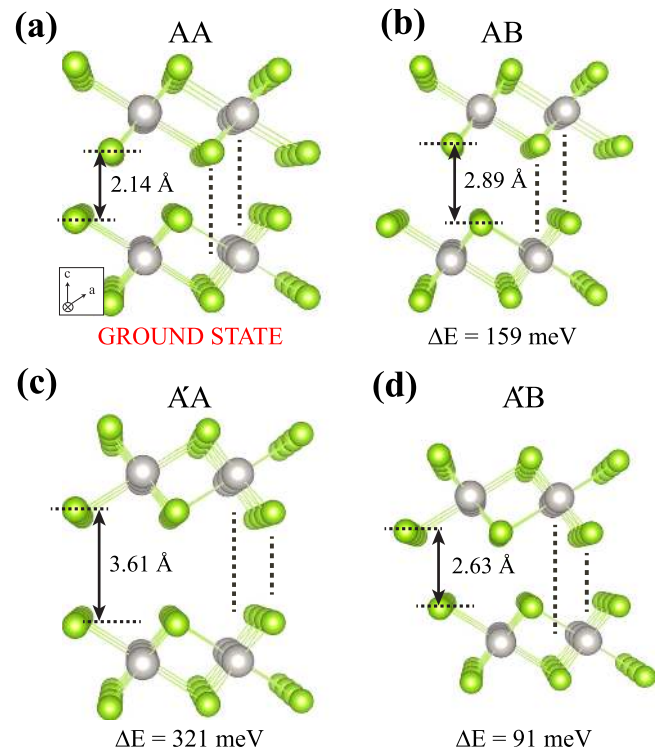


**Figure 3.** Top and side views of crystal structure of bilayer 1T-PtSe<sub>2</sub>; (a) AA, (b) AB (c) A'A, and (d) A'B stacking orders. The ground-state energy differences are given under each stacking type labeled with  $\Delta E$ . Dashed lines indicate axial alignment of the upper and lower layer atoms with respect to each other.

2.63 Å for AA, AB, A'A, and A'B stacking orders, respectively.

It is also seen that while the thickness of single layer PtSe<sub>2</sub> is 2.68 Å, with additional layers the thickness of each single layer is reduced and finally reaches a bulk value of 2.56 Å. Moreover, going from bilayer to bulk, the interlayer distance (vertical vacuum spacing between the adjacent layers) also decreases from 2.14 to 2.07 Å. Apparently, there is an increasing trend in layer-layer interaction in the out-of-plane direction and therefore, as a result of thickness-driven compression, covalent Pt-Se bonds are enlarged. As listed in table 1, the lattice constant of the bilayer, trilayer, four-layer, and bulk structures are found to be 3.73, 3.74, 3.75, and 3.77 Å, respectively. As monolayer PtSe<sub>2</sub>, the ground state structure of the bilayer, trilayer, four-layer, and bulk structures is also found to be nonmagnetic. Therefore, thickness-dependence magnetization is absent in the PtSe<sub>2</sub> structures.

### 4.2. Thickness dependence of electronic properties

In order to determine how the electronic characteristics are modified with an increasing number of layers, we also calculate the electronic band dispersions of monolayer, bilayer, trilayer, and bulk PtSe<sub>2</sub>. As shown in figure 4, going from a monolayer to bilayer structure, the electronic band gap of the material rapidly decreases from 1.17 eV to 0.19 eV and it is also found that PtSe<sub>2</sub> crystals having a thickness larger than two layers all exhibit metallic behavior. In monolayer and

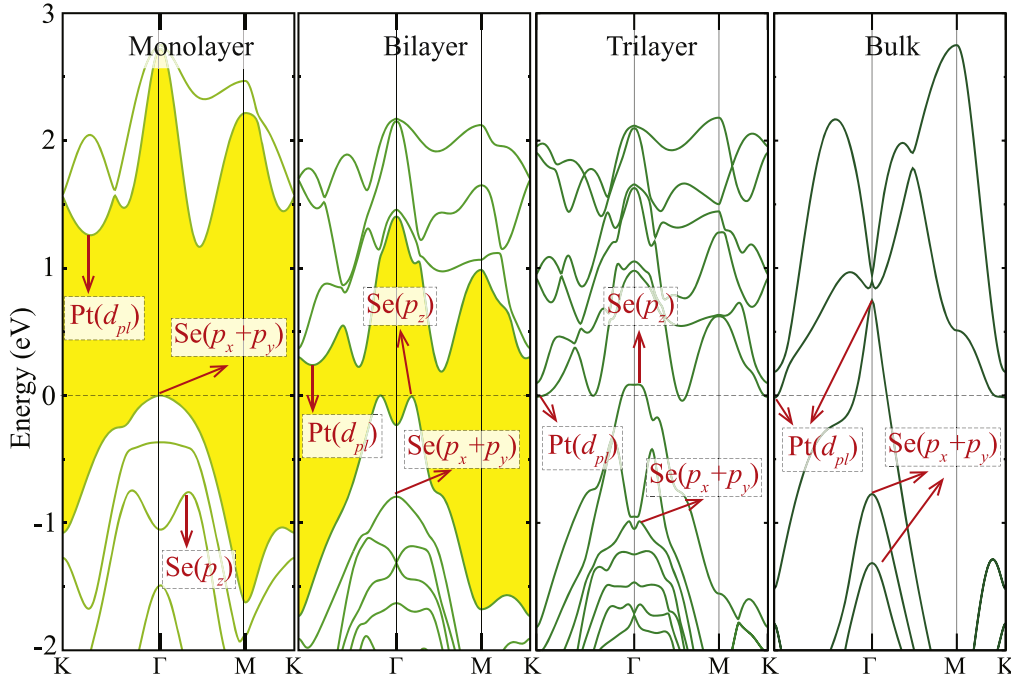


**Figure 4.** The SOC included electronic band dispersions of monolayer, bilayer, trilayer, and bulk 1T-PtSe<sub>2</sub> structures. The Fermi level is set to zero.

**Table 1.** The calculated parameters for the 1T-PtSe<sub>2</sub> structures are; the lattice constants,  $a = b$ ; overall thickness as the uppermost-lowermost Se-Se distance in the unitcell,  $h$ ; the charge donation from Pt to Se atoms,  $\Delta\rho$ ; the cohesive energy per atom,  $E_{Coh}$ ;  $\Phi$  and  $\mu$  are the values of work function and magnetization, respectively;  $E_{gap}$ , the energy band gap of the structure.

	$a = b$ (Å)	$h$ (Å/unitcell)	$\Delta\rho$ ( $e^-$ )	$E_{Coh}$ (eV/atom)	$\Phi$ (eV)	$\mu$ ( $\mu_B$ )	$E_{gap}$ (eV)
1L PtSe <sub>2</sub>	3.70	2.68	0	4.43	5.36	0	1.17
2L PtSe <sub>2</sub>	3.73	7.39	0	4.53	4.64	0	0.19
3L PtSe <sub>2</sub>	3.74	12.04	0	4.57	4.67	0	0
4L PtSe <sub>2</sub>	3.75	16.67	0	4.59	4.72	0	0
Bulk PtSe <sub>2</sub>	3.77	2.56	0	4.65	4.76	0	0

bilayer structures of PtSe<sub>2</sub> the CBM states are composed of  $d$  state electrons that occupy  $d_{xy}$ ,  $d_{yz}$ ,  $d_{xz}$  and  $d_{x^2-y^2}$  orbitals of Pt atom.

While the location of CBM in BZ remains the same (at the  $\Gamma$ -M) when going from monolayer to bilayer, VBM is shifted from the  $\Gamma$  to the K- $\Gamma$  high symmetry point. It is also worth noting that the local minimum energy state of the CBM of the monolayer within the K- $\Gamma$  translocates its position in the Brillouin Zone to the K symmetry point with the effect of additional layers. Rapid decrease in band energy of CB states and increase in VB states leads to metallization starting from trilayer.

On the other hand, the VBM state of the monolayer, that originates from  $p_x$  and  $p_y$  states of Se atoms, changes its energy space and takes position at the states energetically lower than the VBM state of the few-layer PtSe<sub>2</sub>. Moreover, the VBM state of the bilayer, which consists of  $p_z$  orbitals of Se atoms, crosses the Fermi level and becomes one of the metallic transition band at the few-layer PtSe<sub>2</sub>, as seen in the first case the same trend appears in the  $p_z$  orbitals of the Se

atoms. It is obviously seen that the nesting in the corresponding state disappears while the number of layers of PtSe<sub>2</sub> increases.

In addition, the work function values of bilayer, trilayer, four-layer, and bulk structures are found to be 4.64, 4.67, 4.72, and 4.76 eV, respectively. The reason for a sudden decrease from monolayer to bilayer in the work function value is related to the rising of  $p_z$  orbitals of Se atoms from monolayer to bilayer. Then, the increasing work function trend from bilayer to bulk is an expected behavior due to the decrease in surface to bulk ratio of the structure.

#### 4.3. Thickness dependence of vibrational properties

Investigation of the vibrational properties not only allows one to deduce the dynamical stability of the structure but also allows the determination of characteristic properties such as bond strengths, layer thickness and polarizability. In this subsection, thickness dependency of phonon band dispersions, Raman intensities and eigen-frequency shifts of the

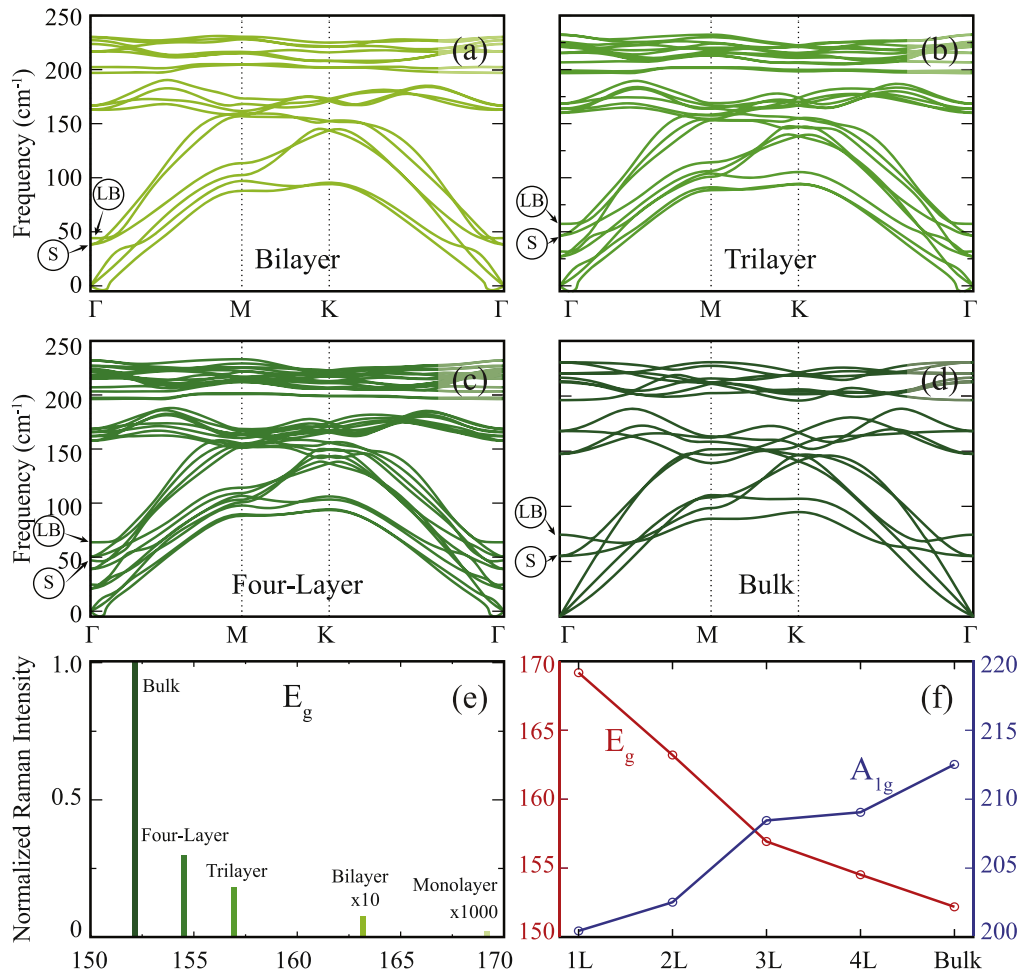


**Figure 5.** The phonon band dispersions of (a) bilayer, (b) trilayer, (c) four-layer and (d) bulk. The S and LB mode frequencies are indicated. (e) Layer dependent Raman intensity of  $E_g$  mode. (f) Frequency shifts of the  $E_g$  and  $A_{1g}$  modes with respect to number of layers. 1L, 2L, 3L and 4L denote monolayer, bilayer, trilayer and four-layer, respectively.

prominent peaks of bilayer, trilayer, four-layer and bulk PtSe<sub>2</sub> are investigated.

Figures 5(a)–(d) show the calculated phonon band structure of bilayer, trilayer, four-layer and bulk PtSe<sub>2</sub>. It is seen that all the phonon modes have real eigenfrequencies, which indicate that bulk and few-layered PtSe<sub>2</sub> are stable. The appearance of small imaginary frequencies (less than  $5 \text{ cm}^{-1}$ ) near the gamma point are not an indication of instability, they are numerical artifacts caused by the inaccuracy of the FFT grid. As shown in figures 5(a)–(d), while LA modes cross the low-frequency optical modes, highest-frequency dispersionless optical modes are well-separated from low-lying phonon branches. Computationally predicted modes at  $152.2$  and  $212.5 \text{ cm}^{-1}$  correspond to the  $E_g$  and  $A_{1g}$  phonons of bulk PtSe<sub>2</sub> and are in good agreement with previous experimental results indicating the reliability of the computational methodology of phonons [49]. As shown in the figure, in addition to the  $E_g$  and  $A_{1g}$  modes of the monolayer structure, additional peaks with low frequencies corresponding to shear (S) and layer-breathing (LB) appear with the increasing thickness. It is found that S and LB modes are Raman active and as the number of layer increases from bilayer to bulk, the

frequencies of S and LB modes increase from  $38.8$  and  $44.0 \text{ cm}^{-1}$  to  $55.0$  and  $74.3 \text{ cm}^{-1}$ , respectively.

It is also worth noting that, as shown in figure 5(e), Raman vibrational characteristics of the  $E_g$  phonon strongly depend on the material thickness. It appears that with increasing thickness, layer-layer interaction originated compression on each sublayer yields two consequences in PtSe<sub>2</sub>; (i) phonon softening due to enlarged Pt-Se bonds and (ii) increasing Raman activity due to enhanced polarizability.

It is also seen from figure 5(f) that when the number of layers is increased, the  $A_{1g}$  peak hardens while the  $E_g$  peak softens. The downshift in the frequency of the  $E_g$  peak is ascribed to the change in the dielectric screening environment for long-range Coulomb interactions as the thickness of the material increases. However, the upshift in the frequency of the  $A_{1g}$  peak is attributed to increasing interlayer interactions which enhance the restoring forces on the atoms [50, 51]. Therefore, the strong layer dependency of Raman intensity of the  $E_g$  mode and peak positions of the  $E_g$  and  $A_{1g}$  modes can be used to determine the material thickness.

## 5. Conclusions

In this study, we investigated thickness dependency of structural, vibrational and electronic properties of 1T-PtSe<sub>2</sub> by performing first-principles calculations. First, it was found that the monolayer of platinum diselenide forms a dynamically stable hexagonal 1T phase, and the monolayer is an indirect band gap semiconductor.

The electronic nature of the monolayer structure changes negligibly under biaxial tensile deformation revealing the robust semiconductor character of the material. In addition, electronic dispersion calculations on crystals of various thickness showed that while monolayer and bilayer structures of 1T-PtSe<sub>2</sub> are indirect band-gap semiconductors, all thicker structures exhibit a metallic character.



The layer-dependent vibrational spectra of the 1T-PtSe<sub>2</sub> structures reveal that Raman active shear mode, layer-breathing mode, E<sub>g</sub> mode, and A<sub>1g</sub> mode display significant shifts indicating the increasing layer-layer interaction. Moreover, the Raman intensity of the E<sub>g</sub> phonon branch is found to be quite sensitive to the material thickness and therefore it can be used for the determination of the number of layers by Raman spectroscopy.

Our study provides an insight into the electronic and vibrational properties of ultra-thin 1T-PtSe<sub>2</sub> materials and also a computational strategy for identifying the number of layers of 1T-PtSe<sub>2</sub> at the atomic scale.

## Acknowledgments

Computational resources were provided by TUBITAK ULAKBIM, High Performance and Grid Computing Center (TR-Grid e-Infrastructure). HS acknowledges financial support from the TUBITAK under the project number 117F095.

## ORCID iDs

A Kandemir  <https://orcid.org/0000-0001-9813-6421>  
 S V Badalov  <https://orcid.org/0000-0002-8481-4161>  
 F Iyikanat  <https://orcid.org/0000-0003-1786-3235>  
 H Sahin  <https://orcid.org/0000-0002-6189-6707>

## References

- [1] Brodie B C 1859 *Philos. Trans. R. Soc. London* **149** 249
- [2] Schuller I K 1980 *Phys. Rev. Lett.* **44** 1597
- [3] Novoselov K S, Geim A K, Morozov S V, Jiang D, Zhang Y, Dubonos S V, Grigorieva I V and Firsov A A 2004 *Science* **306** 666
- [4] Geim A K and Grigorieva I V 2013 *Nature* **499** 419
- [5] Late D J, Liu B, Luo J, Yan A, Matte H S S, Grayson M, Rao C N R and Dravid V P 2012 *Adv. Mater.* **24** 3549
- [6] Joshi S et al 2013 *ACS Nano* **8** 430–42
- [7] Kim K K et al 2012 *Nano Lett.* **12** 161
- [8] Zhuang H L and Hennig R G 2012 *Appl. Phys. Lett.* **101** 153109
- [9] Vogt P, Padova P D, Quaresima C, Avila J, Frantzeskakis E, Asensio M C, Resta A, Ealet B and Lay G L 2012 *Phys. Rev. Lett.* **108** 155501
- [10] Cahangirov S, Topsakal M, Aktürk E, Şahin H and Ciraci S 2009 *Phys. Rev. Lett.* **102** 236804
- [11] Parks G A 1965 *Chem. Rev.* **65** 177
- [12] Khan A I and O'Hare D 2002 *J. Mater. Chem.* **12** 3191
- [13] Akbali B, Yanilmaz A, Tomak A, Tongay S, Çelebi C and Sahin H 2017 *Nanotechnology* **28** 415706
- [14] Ataca C, Şahin H, Aktürk E and Ciraci S 2011 *J. Phys. Chem. C* **115** 3934
- [15] Chhowalla M, Shin H S, Eda G, Li L J, Loh K P and Zhang H 2013 *Nat. Chem.* **5** 263
- [16] Mak K F, Lee C, Hone J, Shan J and Heinz T F 2010 *Phys. Rev. Lett.* **105** 136805
- [17] Zhang Y et al 2014 *Nat. Nanotechnol.* **9** 111
- [18] Castellanos-Gomez A, Poot M, Steele G A, van der Zant H S, Agraït N and Rubio-Bollinger G 2012 *Adv. Mater.* **24** 772
- [19] Wang Q H, Kalantar-Zadeh K, Kis A, Coleman J N and Strano M S 2012 *Nature Nanotech.* **7** 699
- [20] Jariwala D, Sangwan V K, Lauhon L J, Marks T J and Hersam M C 2014 *ACS Nano* **8** 1102
- [21] Tan C and Zhang H 2015 *Chem. Soc. Rev.* **44** 2713
- [22] Qian X, Liu J, Fu L and Li J 2014 *Science* **346** 1344
- [23] Guo G Y and Liang W Y 1986 *J. Phys. C: Solid State Phys.* **19** 995
- [24] Kliche G 1985 *J. Solid State Chem.* **56** 26
- [25] Yeo J S L, Vittal J J, Henderson W and Hor T A 2002 *J. Chem. Soc., Dalton Trans.* **3** 328
- [26] Ullah K, Ye S, Jo S B, Zhu L, Cho K Y and Oh W C 2014 *Ultrason. Sonochem.* **21** 1849
- [27] Ye S and Oh W C 2016 *Mat. Sci. Semicond. Process.* **48** 106
- [28] Wang Y et al 2015 *Nano Lett.* **15** 4013
- [29] Zhao Y, Qiao J, Yu P, Hu Z, Lin Z, Lau S P, Liu Z, Ji W and Chai Y 2016 *Adv. Mater.* **28** 2399
- [30] Du J, Song P, Fang L, Wang T, Wei Z, Li J and Xia C 2018 *Appl. Surf. Sci.* **435** 476
- [31] Li L, Wang W, Chai Y, Li H, Tian M and Zhai T 2017 *Adv. Funct. Mater.* **27** 1701011
- [32] Zhao Y et al 2017 *Adv. Mater.* **29** 1604230
- [33] Chia X, Adriano A, Lazar P, Sofer Z, Luxa J and Pumera M 2016 *Adv. Funct. Mater.* **29** 4306
- [34] Zeng L H et al 2018 *Adv. Funct. Mater.* **1** 1705970
- [35] Zhang Z X, Zeng L H, Tong X W, Gao Y, Xie C, Tsang Y H, Luo L B and Wu Y C 2018 *J. Phys. Chem. Lett.* **9** 1185
- [36] Sattar S and Schwingenschlögl U 2017 *ACS Appl. Mater. Interfaces* **9** 15809
- [37] Sajjad M, Montes E, Singh N and Schwingenschlögl U 2017 *Adv. Mater. Interfaces* **4** 1600911
- [38] Yao W et al 2017 *Nat. Commun.* **8** 14216
- [39] Ciarrocchi A, Avsar A, Ovchinnikov D and Kis A 2018 *Nat. Commun.* **9** 919
- [40] Kresse G and Hafner J 1993 *Phys. Rev. B* **47** 558
- [41] Kresse G and Furthmüller J 1996 *Phys. Rev. B* **54** 11169
- [42] Perdew J P, Burke K and Ernzerhof M 1996 *Phys. Rev. Lett.* **77** 3865
- [43] Grimme S 2006 *J. Comput. Chem.* **27** 1787
- [44] Henkelman G, Arnaldsson A and Jonsson H 2006 *Comput. Mater. Sci.* **36** 354
- [45] Togo A, Oba F and Tanaka I 2008 *Phys. Rev. B* **78** 134106
- [46] Wang Y et al 2015 *Nano Lett.* **15** 4013
- [47] Lee J, Huang J, Sumpter B G and Yoon M 2017 *2D Mater.* **4** 021016
- [48] Gong C, Zhang H, Wang W, Colombo L, Wallace R M and Cho K 2013 *Appl. Phys. Lett.* **103** 053513
- [49] O'Brien M et al 2016 *2D Mater.* **3** 021004
- [50] Lee C, Yan H, Brus L E, Heinz T F, Hone J and Ryu S 2010 *ACS Nano* **4** 2695
- [51] Molina-Sanchez A and Wirtz L 2011 *Phys. Rev. B* **84** 155413